Structural, optical, electrical, and DFT studies of chitosan/polyvinyl alcohol composite doped with mixed nanoparticles (GO/TiO₂) for flexible energy-storage devices

Norah Algethami[1,*]

[1] *Department of Physics, College of Science, Taif University, P. O. Box 11099, Taif 21944, Saudi Arabia*

ABSTRACT

In this current study, the polymer nanocomposites films based on chitosan (Cs)/ polyvinyl alcohol (PVA)/ with graphene oxide (GO) and titanium dioxide (TiO₂) as nanofiller have been prepared by casting technique. The prepared polymer nanocomposites are investigated by using various techniques. The XRD patterns of the studied films revealed a clear decrease in the crystallinity degree of the doped Cs/PVA blend films compared with the pure blend. Due to the existence of OH groups in PVA and NH₂ groups in Cs, the interaction between Cs/PVA mix and GO/TiO₂ nanoparticles occurs and was validated by DFT calculations. This interaction was also linked between the experimental and theoretical findings of DFT calculations. Calculations were made to determine optical properties such as the Urbach energy and energy band gap. As the weight proportion of GO/TiO₂ grows, the energy band gap (indirect and direct) reduces from 5.01 to 5.40 eV for pure blend to 4.46 and 3.49 eV for Blend/ 5%GO/5% TiO₂, and Urbach energy rises. The ionic conductivity of the polymer nanocomposites films was studied by using the AC-impedance spectroscopy. The greater ionic conductivity $\sim 10^{-7}$ S/cm is obtained for the Cs/PVA film, and it was increased to $\sim 10^{-5}$ S/cm at room temperature by adding 5% GO/ 5% TiO₂ nanofiller. It was noted from the dielectric characteristics that the polymer blend with 5% GO/5% TiO₂ added had high dielectric constant values at lower frequencies. The non-Debye behavior was indicated by the incomplete semicircles on the argand plot curves at different concentrations. The improved optical, dielectric, and electrical properties of the Cs/PVA-5%GO/5%TiO₂ nanocomposites make it suitable for use in electronic and optoelectronic devices.

Address correspondence to E-mail: n.alkthamy@tu.edu.sa

1 Introduction

The usefulness of polymer nanocomposites (PNCs) for energy-storage devices in several applications, such as fuel cells, sensors, electrochromic displays, credit cards, batteries, etc., has been thoroughly investigated [1]. A polymer blend, as its name suggests, is a type of material in which at least two polymers combine to produce a new substance with unique physical characteristics. Carefully combining various already-available polymer mixes and fillers can result in very significant potential properties of polymer films. Fascinatingly, doped polymer blend technology allows for the development and fabrication of polymer film composites with performance profiles that cannot be entirely or just partially accomplished by the unblended basic polymers [2–4].The creation and characterization of organic–inorganic nanocomposite for use in various applications have recently attracted much interest. One of the natural, cutting-edge biodegradable polymers, chitosan (Cs, $C_{56}H_{103}N_9O_{39}$) is the second most prevalent amino polysaccharide after cellulose [5]. The CS backbone structure has functional groups for hydroxyl (OH) and amine (NH_2) that make it easier to create covalent connections with a variety of inorganic substances. A lone pair electron is present in the NH_2 group, which also functions as an electron donor for complexation and coordination with the cations of doped nanoparticles. This makes Cs a viable option for Li-ion battery electrolyte films [2, 3]and as a sensor for detecting toxic mercury. The use of Cs in the manufacture of plasmonic metallic nanoparticles (NPs) is another example [4]. The intermolecular contacts between the polymer chains in chitosan and PVA blends have been demonstrated in some investigations to be strong, leading to good biomechanical, structural, and surface characterization [6, 7]. Due to improvements in strength stability, and biocompatibility, mechanical composite films offer benefits over the properties of single components [8]. PVA is a polyhydroxy water soluble polymer that has good hydrophilicity, is non-toxic, and is biocompatible. It also has mechanical resistance and strong chemical. PVA is utilized in a variety of products, including synthetic organs, implants, textiles, contact lenses, medications, films, and cosmetics [9]. Its utilization is crucial for numerous applications, including recycling of polymers and packaging, medication delivery systems, membrane

preparations, and other [10]. Recently, utilizing the function of electron density, the density functional theory method was utilized to characterize the ground state characteristics of materials, including metallic, semiconducting, and insulating materials. As a result, it can be regarded as the most popular and flexible computational physical technique that uses specific functions and basis sets [11]. Pure polymers and polymer blends with the same nominal composition will be characterized using a combination of density functional theory (DFT) and a spectroscopic instrument (FTIR). In this study, we propose to use a mix of ceramic and conducting fillers to demonstrate the synthesis and characterizations of effective flexible dielectric polymeric materials with high ε and low ε''. In order to achieve this, we used a mixture of three-phase nanocomposite films including graphene oxide and TiO_2 as ceramic and conducting fillers in Cs/PVA, respectively. Due to its special characteristics, including high capacitance, water solubility, and the right dielectric strength, Cs/PVA was chosen as the foundation polymer matrix. The addition of fillers that can also act as dopants can change the properties of Cs/PVA [12]. TiO_2 was chosen as a ceramic filler due to its high ε of around 114 at ambient temperature [12]. However, there are drawbacks, such as a lack of mechanical stability [13]. It can outperform the polymer even more if conducting filler is included in addition to ceramic filler. Due to its mechanical strength, conducting properties, simplicity of availability, and practical synthesis procedures, we chose graphene to overcome these restrictions [14, 15]. Based on our knowledge, there is no earlier report on the optical and dielectric characteristics of Cs/PVA-GO/TiO$_2$ nanocomposites films. Due to these important advantages of Cs, PVA, GO, and TiO_2, well investigate the structure, optical, conductivity, and dielectric properties of Cs/PVA-GO/TiO$_2$ nanocomposites films with various concentrations of the GO/TiO$_2$.

2 Experimental techniques

2.1 Materials

Magnetic Stirrer: SH-2 hotplate magnetic stirrer with dual control, 2 L capacity, 100–2000 RPM speed, and a 4.7 × 4.7-inch hot plate with a maximum

temperature of 380 °C, 180 W, and 110 V. Chitosan (Cs) was purchased from Mallinckrodt USA with a deacetylation level of 95%, and an M.W. of 400,000. PVA has molecular weight (MW) = 14,000 Kemphasol, India. Graphene oxide (GO) nanoparticles were purchased from sigma Aldrich Co. USA. Double-distilled water is used for the prepared samples.

2.2 Synthesis of TiO$_2$ nanoparticles

Through the sol–gel method, titanium (IV) tetraisopropoxide [Ti (OCH(CH$_3$)$_2$)$_4$] was diluted in the proper quantity of glacial acetic acid to create the nanoparticles of TiO2. Clear glutinous solution is produced by adding an excessive amount of deionized water. It is then continuously agitated with a magnetic stirrer for five hours. The solution was then left in the dark for 24 h to finish the nucleation process. The solution was then finely ground and calcined at 773 K for 3 h to produce the TiO$_2$ nanoparticles.

2.3 Preparation of polymer nanocomposites films

Solution casting was used to create a blend film of Cs/PVA (70/30 weight percent). In this work, acetic acid (1vol%) was utilized as the solvent 90 ml of acetic acid solution was used to dissolve 1 g of Cs powder for the manufacture of polymer composites. This solution was given with a 30 weight percent PVA addition, and the combination was continually agitated to create a viscous solution. The required quantity of dispersed inorganic GO (5wt.%) and then TiO$_2$ (2, 5, and 8 wt.%) filler were added to Cs/PVA-5% GO solution. The solution was then put into the several dry Petri plates, where it was left to gently evaporate under vacuum for two weeks at room temperature (as shown in Scheme 1). Before the test, the composite polymer nanocomposites films were moved into desiccators for additional drying.

2.4 Characterization techniques

By using a PANalyticalXPert Pro diffractometer with Cu-Kα radiation (k = 1.54178 Å) operated at 40 kV and 30 mA, in the 2θ range of 10–70 at room temperature, the X-ray diffraction experiments were carried out. Using a JASCO (Nicolet iS10, USA) spectrometer, Fourier-transform infrared (FTIR)

spectra of pure Cs/PVA and nanoparticles complexed Cs/PVA films were captured. A JASCO 630 spectrophotometer with an accuracy of ± 0.2 nm was used to study the UV–Vis absorption spectra of a pure Cs/PVA and nanocomposites films at room temperature in the wavelength range of 200–1000 nm. Using a Novocontrol turnkey 40 System with high resolution, broad-band dielectric spectroscopic measurements in the frequency range of 0.1 Hz to 7 MHz were carried out.

## 2.5 Density functional theory (DFT)

DFT: B3LYP/LAN2DZ is used to assess how well theoretical and experimental evidence for the intricate interaction of Cs and PVA correspond. The framework of connection between polymeric matrices is described using theoretical methodology, and agreement degree with experimental evidence for complex interactions between components is calculated (chitosan and polyvinyl alcohol).

3 Results and discussion

3.1 XRD analysis

Figure 1a, b displays the TiO$_2$ and GO nanoparticles XRD pattern, respectively. A typical anatase phase peak can be seen in the TiO$_2$ sample at 2θ = 25.01, 37.95, 47.96, 53.39, 62.60, and 68.84 (JCPDS# 21–1272) [16].

Figure 1c depicts the X-ray diffraction-displayed microstructural changes of the Cs/PVA mix and GO and TiO$_2$ nanoparticle-doped Cs/PVA polymer nanocomposites. In the pure blend, as shown in Fig. 1b, the characteristic peaks of Cs and PVA merged into a broad peak, at 2θ = 19° and 23° with a broad halo [17], due to blending/cross-linking between the CS and PVA [18], which was linked to the polymer blends semi-crystalline nature [19, 20]. The drop in Cs/PVA broad halo intensity indicates an interaction between Cs/PVA and GO/TiO$_2$ ions. This interaction destroys the steric regularity of Cs/PVA blend chains, increasing the degree of amorphousness. The peaks associated with the GO NPs in nanocomposites samples vanish, as seen in Fig. 1c. This suggests that the coordination interactions between the functional groups of Cs/PVA and GO ions, which were confirmed in the research of IR,
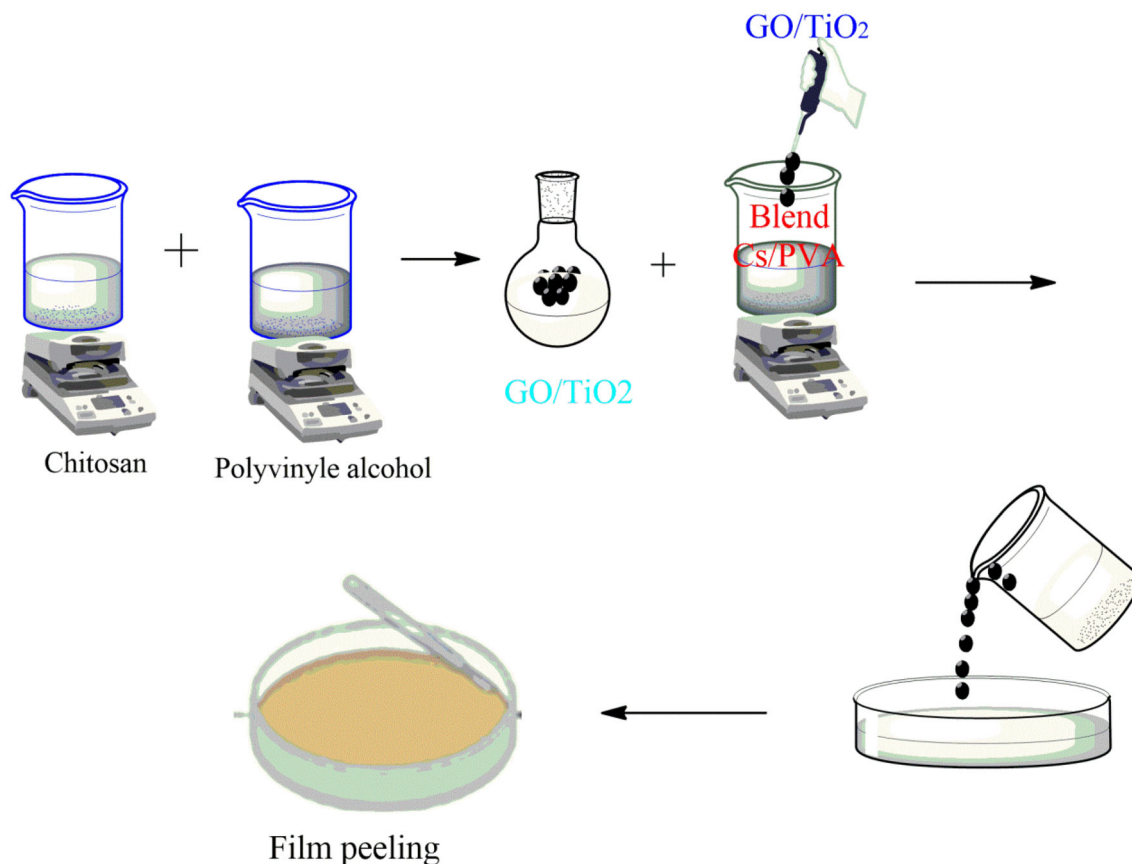
Scheme 1 The preparation process of Cs/PVA-GO/TiO₂nanocomposites films

disturb the order of blend polymer crystallinity. Multiple peaks, an increase in intensity with increasing TiO₂ concentration, and a decrease in the intensity of the characteristic Cs/PVA diffraction peak all point to the existence of TiO₂ as a nanofiller in the polymeric matrices [21]. The nanocomposites have negligibly ($\sim$ 0.1°) distortion in the position of the TiO₂ diffraction peaks, but the intensities change due to the particles dispersion inside the polymeric matrices, which indicates the crystallinity of the composites varies [22]. Additionally, the relation(1) has been used to estimate the crystallinity degree (Xc) from the XRD patterns.

$$Xc = (Sc/S_T) \times 100 \tag{1}$$

where S_T is the total area covered by the XRD patterns and S_c is the region under the crystalline peaks. Table 1 contains the estimated Xc values. It is evident from Table 1 that altering the GO/TiO₂ content in the Cs/PVA blend causes the Xc value to shift or decrease. It should be observed that the nanocomposites' characteristic diffraction peak changed to a lower angle, which in turn indicated a decrease in interplanar spacing. It might be a result of the filler molecules being incorporated into the matrix's interplanar gap [23].

3.2 FTIR and DFT

Figure 2 depicts the FTIR spectra of PVA, Cs, and a mixture of Cs and PVA. The shoulder peak at 2950 cm⁻¹ was attributed to CH₂ asymmetric stretching in the PVA molecules in the hydrogen-bonding state, and the relatively strong vibration band at about 3359 cm⁻¹ corresponded to the symmetrical stretching vibration absorption peak of OH groups on the PVA chains. The characteristic peaks were attributed to the carbonyl group (C=O) stretching vibration, the (CH₂), the (CH + OH) stretching, and the C-O stretching on PVA chains, respectively. The characteristic peaks were 1750, 1433, 1350, and 1035 cm⁻¹ [24], While the three peaks at 1017, 1082, and 1158 cm⁻¹, which were typical peaks of the saccharide structure, could be seen in the

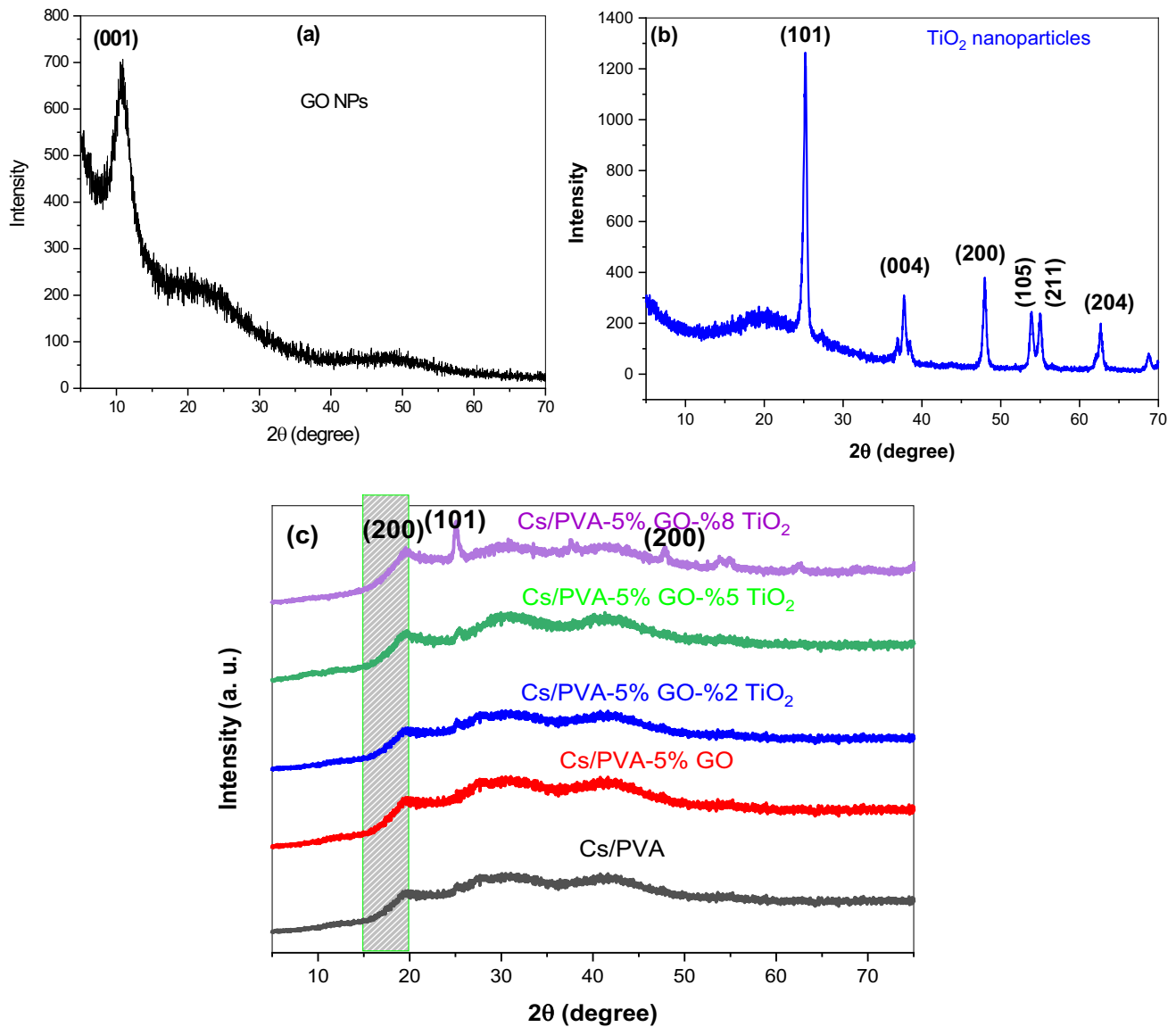Fig. 1 XRD pattern of **a** pure GO NPs, **b** pure TiO$_2$, and **c** pure blend and blend–GO/TiO$_2$ nanocomposites films

Table 1 Degree of crystallinity, optical energy gap (direct and indirect), and Urbach energy (Eu) for the prepared films

Cs/PVA (GO/TiO$_2$ wt. %)	E_g^{in}(eV)	E_g^d(eV)	Eu (eV)	Crystallinity degree (%)
Pure blend	5.01	5.40	0.31477 ± 9.65682E-4	38.23
Blend/5%GO	4.73	5.17	0.43533 ± 0.00326	32.65
Blend/5%GO/2%TiO$_2$	4.77	4.96	0.64593 ± 0.00287	22.98
Blend/5%GO/5%TiO$_2$	3.49	4.46	0.90355 ± 0.00248	15.16
Blend/5%GO/8%TiO$_2$	3.79	4.89	0.77855 ± 0.00248	20.45

FTIR spectrum of the chitosan as shown in Fig. 2. It was determined that the polysaccharides O- and N–H stretching vibrations have a large peak at 3445 cm^{-1}. When amide absorption peaks appeared at 1646 and 1380 cm-1, it was clear that chitosan had a very high degree of deacetylation [18, 25]. The ability to join the chains via hydrogen bonds is made feasible by the carbonyl group groups and −OH found in PVA as well as −OH and -NH$_2$ in chitosan. Due to hydrogen bonding between functional groups,
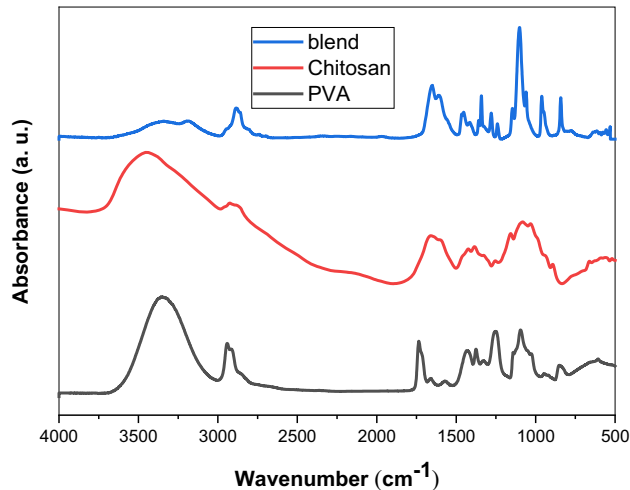
Fig. 2 FTIR spectra of pure PVA, pure Cs, and Cs/PVA blend

changes in the distinctive shape of component spectra, as well as minor shifts in absorption peaks, were noticed. Thus, the blend under study is capable of experiencing both intramolecular and intermolecular interactions.

The intensity of the peaks decreases and the clearly shifted peaks indicate the formation of strong intermolecular hydrogen bonding between the -NH$_2$ group of the Cs and the C=O and −OH groups of the PVA in the Cs/PVA blend when compared to the pure polymers. As shown in Scheme 2, the hydrogen bonds between the -NH$_2$ group of Cs and the C=O and −OH for PVA may facilitate intramolecular interactions between the two polymers [26, 27]. This conclusion is proven using DFT calculations, where the simulated IR spectrum generated by DFT is better in line with the IR experimental spectrum as seen in Fig. 3. This implies that within the polymer mix, the two polymers are more miscible and compatible. The simulated IR was conducted on one monomer in the gaseous phase, but the FTIR absorption spectra were acquired in the solid state, which may account for any shifts observed between the experimental and theoretical FTIR spectra (wavenumbers) of the IR vibration modes [28].

Figure 4 illustrates the FTIR absorption spectra of Cs/PVA blend and nanocomposites samples with various GO/TiO$_2$ NPs concentrations. The obtained spectrum reveals stretching vibrations of the N–H group and a broad band at 3402–3190 cm^{-1} ascribed to the O–H groups. The peaks at 1669, 1560, 1320, and 1081 cm^{-1} are caused by the stretching of the C = O bond, the secondary amide, the tertiary amide, and

the C–O–C stretching vibration of the saccharide structure, respectively. Asymmetric stretching vibration of aliphatic C-H is shown at 2934–2867 cm^{-1} [29]. With the addition of GO/TiO$_2$ NPs, a band at 675 cm^{-1} in Cs/PVA doped with that material almost completely vanishes. With the inclusion of GO/TiO$_2$ NPs, there is also a discernible reduction in the intensities of all bands, and a shifting of some bands to higher or lower wavenumbers, due to the miscibility and complexation between Cs/PVA and GO/TiO$_2$ NPs. These findings could help explain why different compositions of polymer electrolytes have varying ionic conductivity values. Scheme 2 suggests mechanism interaction between GO/TiO$_2$ and Cs/PVA system. In order to form the polymer nanocomposites films, GO/TiO$_2$ may be introduced into the Cs/PVA mixture at the dotted lines in the NH$_2$ of Cs and the C=O and OH groups of PVA in Scheme 2.

3.3 Optical studies

The quickest and easiest way to learn about a materials band structure is to measure its absorption spectra. In the process of absorption, a photon of known energy from the transmitting radiation is absorbed, which excites an electron from a lower to higher energy state. UV–Vis spectra of pure blend and blend doped with various concentrations of GO/TiO$_2$ NPs are shown in Fig. 5 and show peaks associated with the carbonyl groups π–π*electronic transition at 290 nm [30]. For the nanocomposites compared to pure Cs/PVA, the polaron–bipolaron absorption peak is seen to be red shifted; this suggests increased electrical conductivity as has been observed in the current situation and will be discussed in the next section. According to the Taucs model (Eq. 2), the optical band gap is determined from UV–Vis spectra [31]:

$$\alpha h v = A(h v - E g)^n \tag{2}$$

where "n" is 2 and 1/2 for a direct and indirect transition, "α" is the absorption coefficient, "h" is the Plancks constant, "v" is the frequency of light, "Eg" is the band gap, and "A" is a constant. According to Fig. 6a, b and Table 1, which is consistent with the XRD findings, the optical band gap reduced as the fraction of GO/TiO$_2$ increased. According to the XRD finding, the decrease in the Cs/PVA band gap was connected to the changes in the matrix disorder [32].
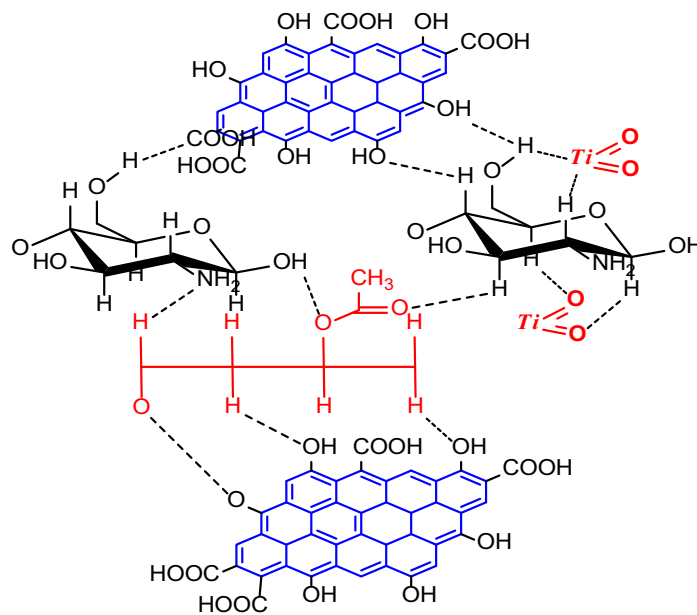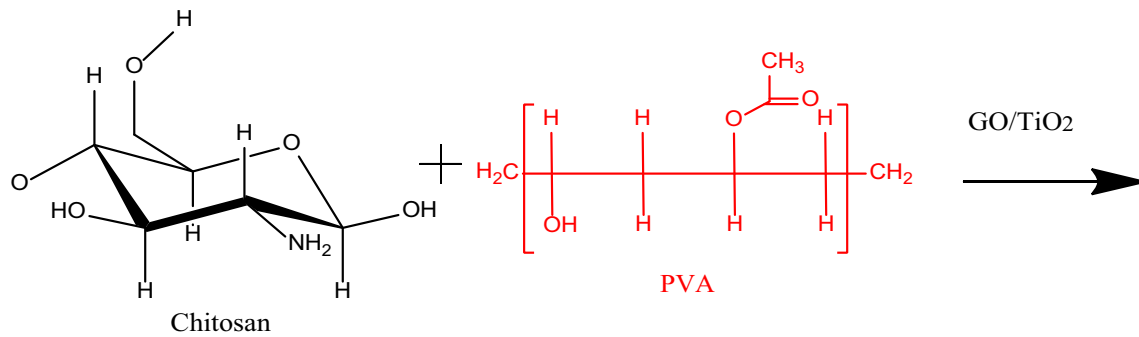
Scheme 2 Suggested mechanism for interaction between Cs/PVA blend and GO/TiO$_2$

Additionally, the main cause of the decrease in the forbidden band is the flaws brought on by the electrical localized states (band tail). Furthermore, due to the trap levels inside the band between LUMO and HOMO of the blend matrix, the decrease in the bandgaps value was linked to the complex development of charge transfer [33], which made the energy necessary for the electron transfer less. This effectively implies that the chains of GO/TiO$_2$ and Cs/PVA are miscible. Additionally, it occurs primarily as a result of the interaction between GO/TiO$_2$ and Cs/PVA, which enhances electron delocalization along Cs/PVA chains. Therefore, for the composites with increasing percentages of GO/TiO$_2$ which have been found here, an increasing trend in electrical conductivity is expected. The increase of the energy gap

value at Blend/5%GO/8%TiO$_2$ nanocomposite was observed compared with the Blend/5%GO/5%TiO$_2$ nanocomposite film due to the increase of the degree of the polymer sample structural ordering. Matching to the XRD results, the energy gap value at Blend/5%GO/5%TiO$_2$ was found to be lower than the values of other concentrations. The exponential relationship between the photon energy (hυ) and absorption coefficient α(υ) close to the absorption edge (Urbach relationship), which is utilized to calculate the localized states width (Urbach energy), is employed by Eq. 3 [34]:

$$\alpha = \alpha_o e^{(hv/Eu)}. \tag{3}$$

Following the completion of the linear fitting (1/slope), as shown in Fig. 7, the Eu value for each
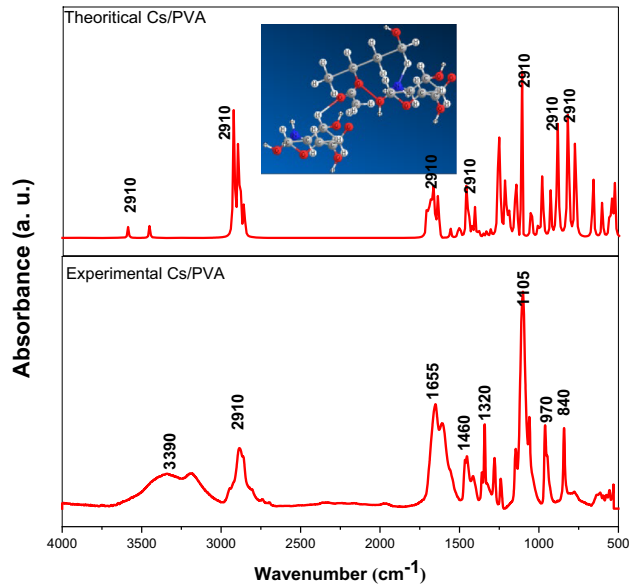
Fig. 3 Experimental and theoretical FTIR spectra of Cs/PVA blend film (the optimized geometry structure of Cs/PVA blend is shown in the inset)
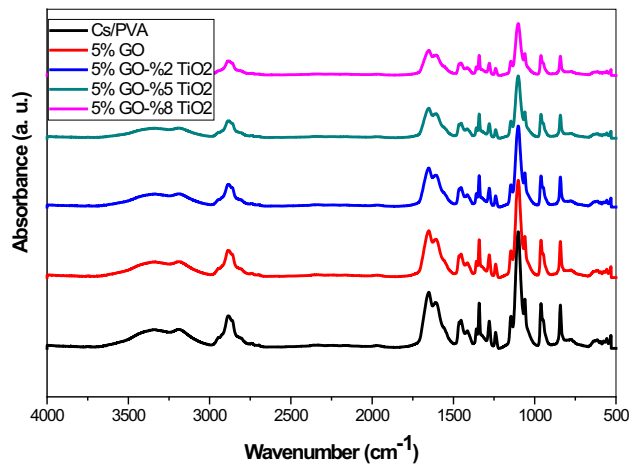

Fig. 4 FTIR spectra of Cs/PVA blend and the Cs/PVA-GO/TiO$_2$ nanocomposites films

sample is recorded in Table 1. Eu increased from 0.31477 eV for Cs/PVA to 0.90355 eV for blend–5%GO/5%TiO$_2$. The transition band gap changes with these values in an inverse manner. We can interpret this outcome as a result of the GO/TiO$_2$ NPs inclusion, which led to structural alterations in the blend matrix and changed the disorder of the Cs/PVA blend chains [35]. The addition of GO/TiO$_2$ NPs caused the Cs/PVA chains defects, which led to the change in Eu. Particularly, the redistribution to the band states caused by the GO/TiO$_2$ nanoparticles
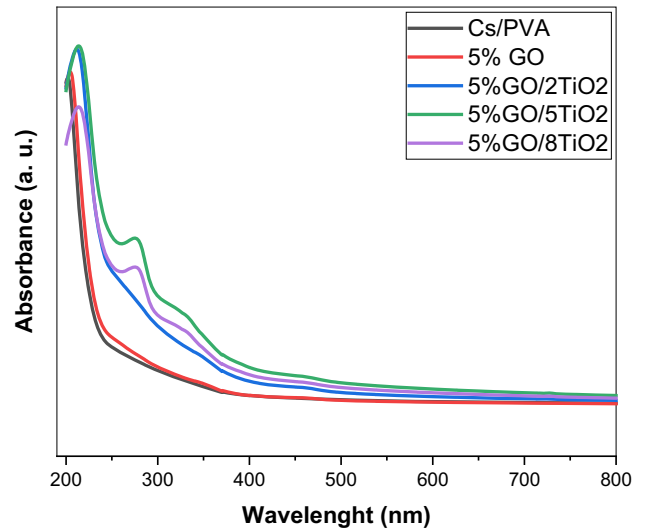

Fig. 5 UV–Vis absorption spectra of pure blend and the blend–GO/TiO$_2$ nanocomposites

results in more tail-to-tail transitions and a modification in the band gap [30].

3.4 Electrical properties

3.4.1 AC conductivity

Figure 8 illustrates the AC electrical conductivity of pure blend and blend doped with various concentrations of GO/TiO$_2$ nanoparticles at different frequencies. The figure shows that at all frequencies tested, the AC conductivity of the nanocomposites films progressively improves with the addition of GO/TiO$_2$ nanoparticles up to a 5%GO/5%TiO$_2$ wt.% loading. The conductivity is found to diminish after this loading. The creation of the charge-transfer complex [36] and a decline in the crystallinity percentage of the Cs/PVA polymer blend sample were both suggested as the causes of the large increase in conductivity that occur with the inclusion of GO/TiO$_2$ NPs in the nanocomposites [37]. Additionally, as the filler content rises, the compactness rises as well, linking the conductive phases via filler network creation. A combination of these conductive connections and a higher chance of charge carriers hopping result in improved conductivity [38]. The shorter conductive paths may be to blame for the slower enhancement of conductivity in the higher frequency band [38]. According to Shuhaimi et al. [39]. the rise in ionic conductivity of the MC-PVA:NH$_4$NO$_3$ polymer electrolytes, with an increase in the AC
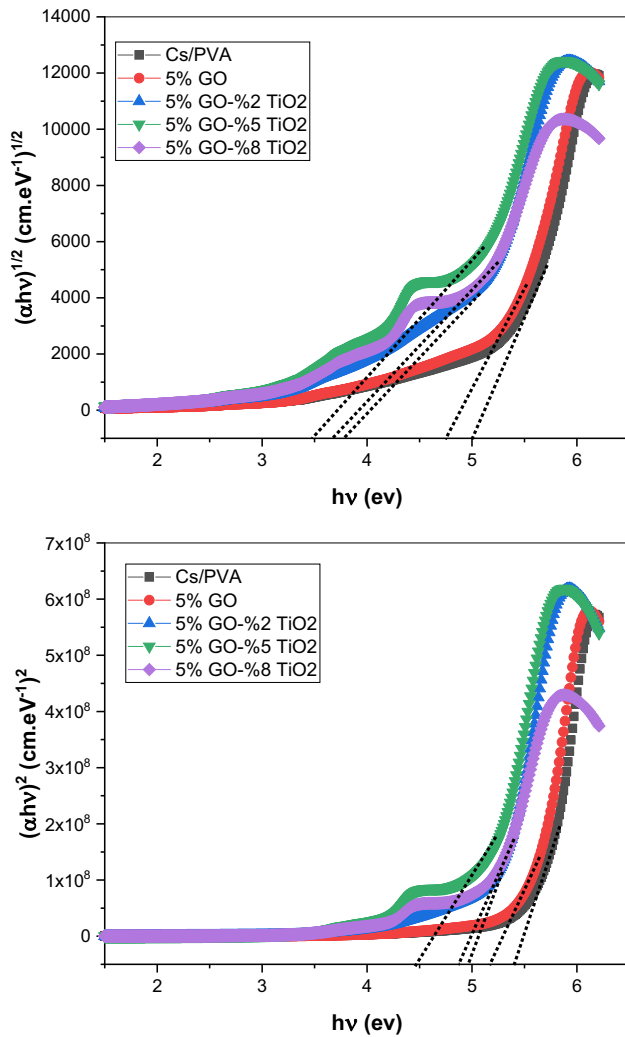
Fig. 6 Variation of $(\alpha h\upsilon)^{1/2}$ and $(\alpha h\upsilon)^2$ versus $(h\upsilon)$ of pure blend and the blend–GO/TiO$_2$ nanocomposites

Fig.7 The relation between Ln(α) vs. ($h\upsilon$) for of blend and the blend–GO/TiO$_2$ nanocomposites
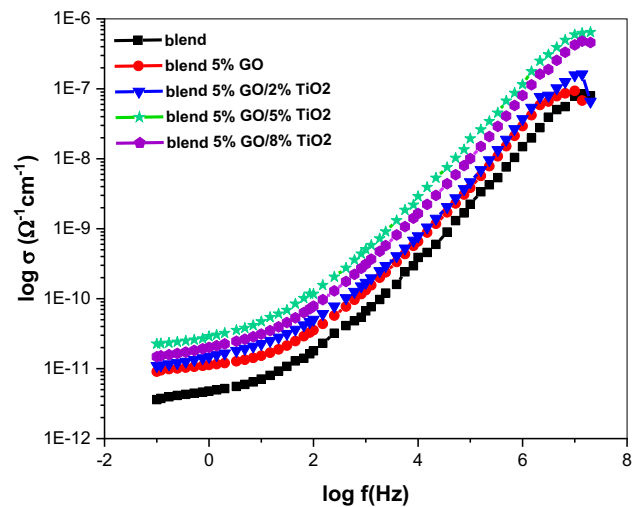
Fig. 8 AC conductivity for pure blend and the blend–GO/TiO$_2$ nanocomposites at room temperature

3.4.2 Dielectric constant

The dielectric characteristic can be utilized as a sign to establish that raise in number of free mobile ions or charge carriers is what is causing the conductivity to increase. For the pure mix and the nanocomposites films, the dielectric constant (real ε' and imaginary ε'') values are determined as follows [43]:

$$\varepsilon' = \frac{Ct}{\varepsilon_o A}, \qquad (4)$$

$$\varepsilon'' = \frac{\sigma}{\varepsilon_o \omega}, \qquad (5)$$

conductivity of the nanocomposites, increases steadily with the addition of filler content, which is connected to the rise in the number density of mobile charge carriers. Filler characteristics like filler aggregation propensy and surface area, and filler conductivity, filler dispersion in the polymer, size, and shape of fillers have a considerable impact on the conductivity of polymeric systems. A homogeneous distribution of nanoparticles in the polymer blend matrix may be ensured at lower filler particle loadings, and these results in a conductive network topology [40]. The agglomeration of nanoparticles, however, decreases the fillers effective surface area with greater loadings of nanoparticles [41]. Because of this, the interfacial area is less, which lowers conductivity [42].
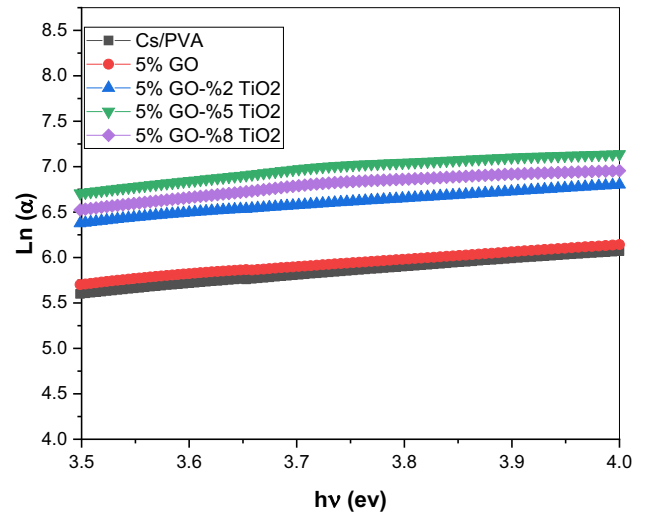
where ε_o is the permittivity of empty space and C is the measured capacitance in parallel mode. Figure 9 shows the ε' and ε'' of a Cs/PVA blend with various GO/TiO$_2$ nanoparticle concentrations at room temperature. The dielectric response is greatest at the lowest frequency, tends to drop, and then becomes constant as the frequency rises, while the conductivity rises. The filling of voids may be the reason why the magnitude of the dielectric constant at low frequency is increased with the quantity of GO/TiO$_2$ nanoparticles. The conductive phase of the polymer matrix started to join and form the conductive network where the dielectric constant increased suddenly as the GO/TiO$_2$ content rose. Due to the electrical relaxation phenomenon, a drop in the ε' and ε'' is observed as the applied frequency rises [44].
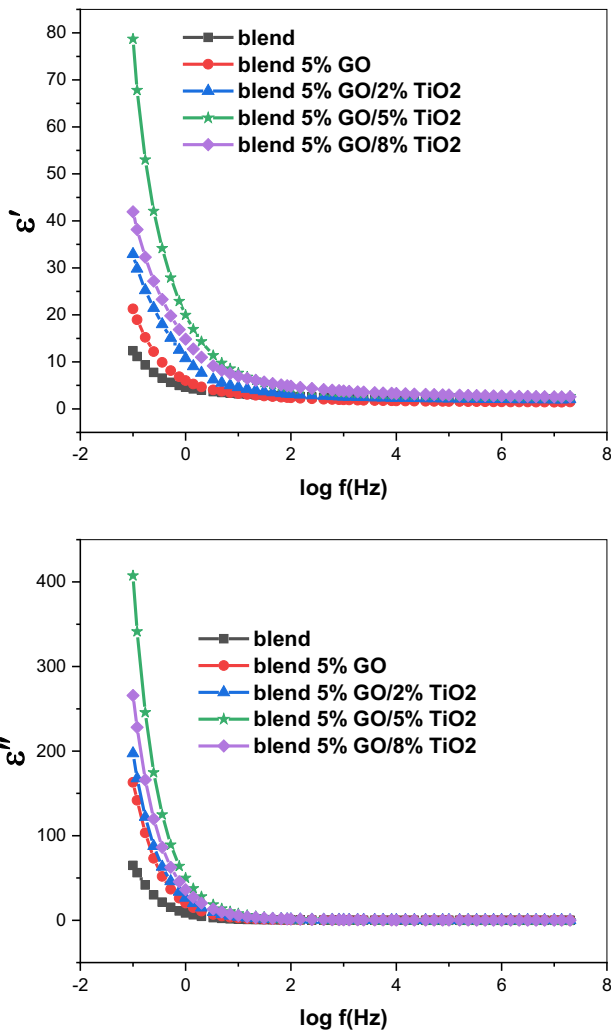

Fig. 9 Dielectric plots ε' and ε'' of pure blend and the blend–GO/TiO$_2$ nanocomposites at room temperature

Molecules and dipoles have enough time at low frequencies to align themselves with the applied field, leading to a high value for the dielectric constant. The dependency of the dielectric constant on the amount of nanofiller, however, tends to be lessened at high frequencies because the dipoles and molecules cannot keep up with the change in electrical field frequency. All polymer composites with conducting or semiconducting additives exhibit this behavior by nature. The interfacial polarization, which mostly results from the passage of charge carriers from one end to the other end, is the primary cause of the higher conductivity of nanocomposites. As a result, the interfaces experience a differential charge accumulation [45]. The local electron displacement causes greater polarization in the combined nanocomposites due to interfacial interactions. This indicates that the polarization created in the polymeric matrices by the application of an electric field is directly proportional to the dielectric values. It is also obvious from Fig. 9 that the ε' and ε'' decreased at blend/ 5%GO/8%TiO$_2$ compared with that of the blend/5% GO/5% TiO$_2$, this may be due to the heterogeneous distribution of GO and TiO$_2$ which allows the charge carriers to get trapped against the defect sites.

3.4.3 Argand plot or complex modulus study

Additionally, the relaxation process in polymer nanocomposites is generated by conductivity of ionic and is represented by the Argand plot. The following equations can be utilized to express the electric modulus M* [22]:

$$M^* = 1/\varepsilon^* = M' + iM''. \tag{6}$$

The dielectric modulus real and imaginary components are determined by using Eqs. 7 and 8.

$$M' = \varepsilon'/\varepsilon'^2 + \varepsilon''^2, \tag{7}$$

$$M'' = \varepsilon''/\varepsilon'^2 + \varepsilon''^2, \tag{8}$$

where M' is the electrical modulus real part and M'' is its imaginary part. In Fig. 10, the Argand plot for polymer nanocomposites is depicted between M' and M'' at room temperature. The polymer generally deviates from its semicircular shape and displays a dispersion of relaxation time. The observed incomplete semicircle curves in this image demonstrate non-Debye nature. Numerous types of polarization, the relaxation mechanism, and numerous
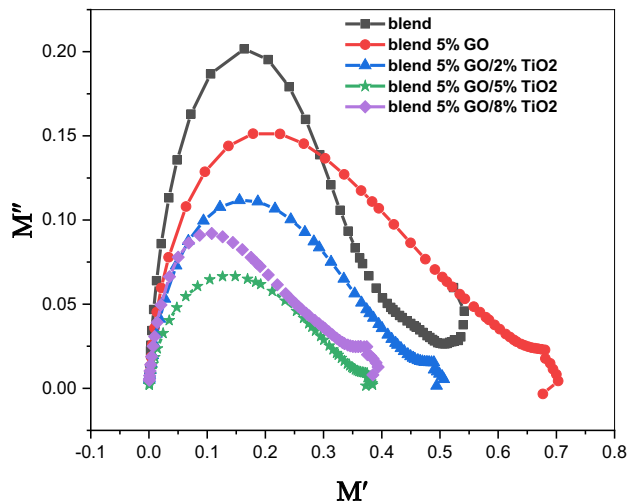
Fig. 10 Complex modulus plot for pure blend and the blend–GO/TiO$_2$ nanocomposites at room temperature

interactions between the ions and the dipoles all contribute to the non-Debye behavior [46]. It is widely known that the conductivity of polymer nanocomposites is closely related to the arcs radius [47]. When the concentration of nanoparticles in polymer nanocomposites increases, the radius of the arc decreases, indicating an increase in conductivity [48]. In Fig. 10, it is clear that as the content of GO/TiO$_2$ NPs in the polymer nanocomposites increases, the length of the arc shortens, indicating an increase in conductivity. This work further confirms that the polymer nanocomposites with 5% GO/5%TiO$_2$ nanoparticles added achieve a greater conductivity than other compositions.

4 Conclusion

The solution-casting process was used to create pure Cs/PVA, Cs/PVA-5%GO, and varied (2, 5, 8) wt.% TiO$_2$-filled Cs/PVA-5%GO polymeric nanocomposites. The optical, conductivity, and dielectric properties with combined FTIR/DFT of the films were investigated. According to XRD results, the virgin Cs/PVA blend with GO/TiO$_2$ NPs added increases the amount of amorphous domains in polymer nanocomposites films. The interaction between Cs and PVA was confirmed by DFT calculations as well as FTIR experimental spectrum. The hydrogen bonds between the NH$_2$ group in Cs and the OH group in PVA result in a connection within the polymer mixture. This interaction suggests that the mixture is compatible and miscible within the Cs/PVA mixture. Due to changes in the matrix disorder of the polymers, the predicted Eg values of all samples decreased as GO/TiO$_2$ content rose. The addition of GO/TiO$_2$ results in an increase in the Urbach energy (Eu) of the PNCs, which is correlated for a significant number of potential tail-to-tail transitions. With increased GO/TiO$_2$ doping in Cs/PVA nanocomposite films at room temperature, the ionic conductivity is improved. The Cs/PVA nanocomposites with 5%GO/5%TiO$_2$ doping exhibit good optical characteristics and high conductivity among the produced samples. The Maxwell–Wagner model, which accounts for the polarization of dipoles or charges, predicts a drop in the dielectric constant and a corresponding increase in dielectric loss with frequency. According to measurements of the dielectric properties, adding GO/TiO$_2$ to the Cs/PVA matrix makes it easier to optimize the dielectric qualities. In order to be used in electronic applications such as separators in batteries, storage devices, and thermoelectric devices, the current polymer nanocomposites had to meet the necessary optical, conductivity, and dielectric properties. This merits additional study.

Author contributions

NA: Investigation, conceptualization, methodology, original draft, formal analysis, writing—review and editing.

Funding

The authors have not disclosed any funding.

Data availability

The authors confirm that the data supporting the findings of this study are available within the article.

Declarations

Conflicts of interest The authors declare that they have no conflict of interest.

Ethical approval The authors have found all the moral standards and will intended to follow them in future.

References

1. M. Kang, M. Wang, S. Zhang, X. Dong, L. He, Y. Zhang et al., Highly selective and sensitive reversible sensor for Cu (II) detection based on hollow TiO2 spheres modified by fluorescein hydrozine-3, 6-diacetic acid. Electrochimica Acta **161**, 186–194 (2015)

2. J. Wang, S. Song, S. Gao, R. Muchakayala, R. Liu, Q. Ma, Mg-ion conducting gel polymer electrolyte membranes containing biodegradable chitosan: preparation, structural, electrical and electrochemical properties. Polym. Test. **62**, 278–286 (2017)

3. S. Mafirad, M.R. Mehrnia, P. Zahedi, S.N. Hosseini, Chitosan-based nanocomposite membranes with improved properties: effect of cellulose acetate blending and TiO2 nanoparticles incorporation. Polym. Compos. **39**(12), 4452–4466 (2018)

4. A.M. El Sayed, A.D.M. Mohamad, Synthesis, structural, thermal, optical and dielectric properties of chitosan biopolymer; influence of PVP and α-Fe2O3 Nanorods. J. Polym. Res. **25**(8), 1–14 (2018)

5. G.B. Patel, N.L. Singh, F. Singh, Modification of chitosan-based biodegradable polymer by irradiation with MeV ions for electrolyte applications. Mater. Sci. Eng., B **225**, 150–159 (2017)

6. J.M. Yang, W.Y. Su, M.C. Yang, Evaluation of chitosan/PVA blended hydrogel membranes. J. Membr. Sci. **236**(1–2), 39–51 (2004)

7. E. de Souza Costa-Júnior, M.M. Pereira, H.S. Mansur, Properties and biocompatibility of chitosan films modified by blending with PVA and chemically crosslinked. J. Mater. Sci.: Mater. Med. **20**(2), 553–561 (2009)

8. M.M. Abutalib, A. Rajeh, Structural, thermal, optical and conductivity studies of Co/ZnO nanoparticles doped CMC polymer for solid state battery applications. Polym. Test. **91**, 106803 (2020)

9. R. Niranjan, M. Kaushik, J. Prakash, K.S. Venkataprasanna, C. Arpana, P. Balashanmugam, G.D. Venkatasubbu, Enhanced wound healing by PVA/Chitosan/Curcumin patches: in vitro and in vivo study. Colloids Surf. B **182**, 11 (2019)

10. A. Abraham, P.A. Soloman, V.O. Rejini, Preparation of chitosan-polyvinyl alcohol blends and studies on thermal and mechanical properties. Procedia Technol. **24**, 741–748 (2016)

11. W. Kohn, L.J. Sham, Self-consistent equations including exchange and correlation effects. Phys. Rev. **140**(4A), A1133 (1965)

12. S. Ishaq, F. Kanwal, S. Atiq, M. Moussa, U. Azhar, I. Gul, D. Losic, Dielectric and impedance spectroscopic studies of three phase graphene/titania/poly (vinyl alcohol) nanocomposite films. Results Phys. **11**, 540–548 (2018)

13. G.K. Goh, S.K. Donthu, P.K. Pallathadka, Cracking and orientation of solution-deposited rutile TiO2 films. Chem. Mater. **16**(15), 2857–2861 (2004)

14. C. Lee, X. Wei, J.W. Kysar, J. Hone, Measurement of the elastic properties and intrinsic strength of monolayer graphene. Science **321**(5887), 385–388 (2008)

15. A.A. Balandin, S. Ghosh, W. Bao, I. Calizo, D. Teweldebrhan, F. Miao, C.N. Lau, Superior thermal conductivity of single-layer graphene. Nano Lett. **8**(3), 902–907 (2008)

16. S.M. Hassan, A.I. Ahmed, M.A. Mannaa, Preparation and characterization of SnO2 doped TiO2 nanoparticles: Effect of phase changes on the photocatalytic and catalytic activity. J. Sci.: Adv. Mater. Devices **4**(3), 400–412 (2019)

17. A.M. Hezma, A. Rajeh, M.A. Mannaa, An insight into the effect of zinc oxide nanoparticles on the structural, thermal, mechanical properties and antimicrobial activity of Cs/PVA composite. Colloids Surf A: Physicochem. Eng. Aspe **581**, 123821 (2019)

18. D.C. Bharati, P. Rawat, A.L. Saroj, Structural, thermal, and ion dynamics studies of PVA-CS-NaI-based biopolymer electrolyte films. J. Solid State Electrochem. **25**(6), 1727–1741 (2021)

19. F.M. Ali, R.M. Kershi, M.A. Sayed, Y.M. AbouDeif, Evaluation of structural and optical properties of Ce3+ ions doped (PVA/PVP) composite films for new organic semiconductors. Physica B **538**, 160–166 (2018)

20. A.M. Shehap, D.S. Akil, Structural and optical properties of TiO2 nanoparticles/PVA for different composites thin films. Int. J. Nanoelectron. Mater. **9**, 17–36 (2016)

21. M. Hdidar, S. Chouikhi, A. Fattoum, M. Arous, A. Kallel, Influence of TiO2 rutile doping on the thermal and dielectric properties of nanocomposite films based PVA. J. Alloy. Compd. **750**, 375–383 (2018)

22. V. Hebbar, R.F. Bhajantri, J. Naik, Physico-chemical properties of Bismuth nitrate filled PVA–LiClO4 polymer composites for energy storage applications. J. Mater. Sci.: Mater. Electron. **28**(8), 5827–5839 (2017)

23. R. Chen, M.H. So, C.M. Che, H. Sun, Controlled synthesis of high crystalline bismuth sulfide nanorods: using bismuth citrate as a precursor. J. Mater. Chem. **15**(42), 4540–4545 (2005)

24. A. Tawansi, A. El-Khodary, M.M. Abdelnaby, A study of the physical properties of FeCl3 filled PVA. Curr. Appl. Phys. **5**(6), 572–578 (2005)

25. T. Hoang, K. Ramadass, T.T. Loc, T.T. Mai, L.D. Giang, V.V. Thang et al., Novel drug delivery system based on ginsenoside Rb1 loaded to chitosan/alginate nanocomposite films. J. Nanosci. Nanotechnol. **19**(6), 3293–3300 (2019)

26. S. Chapi, H. Devendrappa, Optical, electrical, thermal and electrochemical studies of spin-coated polyblend-ZnO nanocomposites. J. Mater. Sci.: Mater. Electron. **27**(11), 11974–11985 (2016)

27. S. Chapi, Enhanced electrochemical, structural, optical, thermal stability and ionic conductivity of (PEO/PVP) polymer blend electrolyte for electrochemical applications. Ionics **22**(6), 803–814 (2016)

28. A.A. Al-Muntaser, M.M. El-Nahass, H.A. Saad, DFT calculation and experimental study on electronic structure and optical properties of 7-Amino-4-oxo-3-(2-(2-thienyl) vinyl)-4H, 8H- [1, 2, 4] triazino [3, 4-b] [1, 3, 4] thiadiazine-8-carbonitrile thinfilms. Optik **220**, 165199 (2020)

29. J. Bonilla, E.L.E.N.A. Fortunati, L. Atarés, A. Chiralt, J.M. Kenny, Physical, structural and antimicrobial properties of poly vinyl alcohol–chitosan biodegradable films. Food Hydrocolloids **35**, 463–470 (2014)

30. H.E. Ali, H.S. Abd-Rabboh, N.S. Awwad, H. Algarni, M.A. Sayed, A.F. Abd El-Rehim et al., Photoluminescence, optical limiting, and linear/nonlinear optical parameters of PVP/PVAL blend embedded with silver nitrate. Optik **247**, 167863 (2021)

31. M.M. Abutalib, Insights into the structural, optical, thermal, dielectric, and electrical properties of PMMA/PANI loaded with graphene oxide nanoparticles. Phys. B Condens. Matter. **552**, 19–29 (2019)

32. S. Awad, S. El-Gamal, A.M. El Sayed, E.E. Abdel-Hady, Characterization, optical, and nanoscale free volume properties of Na-CMC/PAM/CNT nanocomposites. Polym. Adv. Technol. **31**(1), 114–125 (2020)

33. M.M. Abutalib, A. Rajeh, Influence of MWCNTs/Li-doped TiO2 nanoparticles on the structural, thermal, electrical and mechanical properties of poly (ethylene oxide)/poly (methylmethacrylate) composite. J. Organomet. Chem. **918**, 121309 (2020)

34. H.M. Alghamdi, A. Rajeh, Synthesis of carbon nanotubes/titanium dioxide and study of its effect on the optical, dielectric, and mechanical properties of polyvinyl alcohol/sodium alginate for energy storage devices. Int. J. Energy Res. (2021). https://doi.org/10.1002/er.7578

35. A. Abdel-Galil, M.R. Balboul, A. Atta, I.S. Yahia, A. Sharaf, Preparation, structural and optical characterization of nanocrystalline CdS thin film. Physica B **447**, 35–41 (2014)

36. S. Sivadevi, S. Selvasekarapandian, S. Karthikeyan, C. Sanjeeviraja, H. Nithya, Y. Iwai, J. Kawamura, Proton-conducting polymer electrolyte based on PVA-PAN blend doped with ammonium thiocyanate. Ionics **21**(4), 1017–1029 (2015)

37. N. Algethami, A. Rajeh, H.M. Ragab, A.E. Tarabiah, F. Gami, Characterization, optical, and electrical properties of chitosan/polyacrylamide blend doped silver nanoparticles. J. Mater. Sci.: Mater. Electron. **33**(13), 10645–10656 (2022)

38. V. Hebbar, R.F. Bhajantri, Synthesis and dielectric investigations of bismuth sulfide particles filled PVA: polypyrrole core-shell nanocomposites. Mater. Sci. Eng., B **224**, 171–180 (2017)

39. N.E.A. Shuhaimi, N.A. Alias, M.Z. Kufian, S.R. Majid, A.K. Arof, Characteristics of methyl cellulose-NH4NO3-PEG electrolyte and application in fuel cells. J. Solid State Electrochem. **14**(12), 2153–2159 (2010)

40. H.M. Alghamdi, M.M. Abutalib, A. Rajeh, M.A. Mannaa, O. Nur, E.M. Abdelrazek, Effect of the Fe2O3/TiO2 nanoparticles on the structural, mechanical, electrical properties and antibacterial activity of the biodegradable chitosan/polyvinyl alcohol blend for food packaging. J. Polym. Environ. **30**(3865–3874), 1–10 (2022)

41. S. Mehraj, M.S. Ansari, Structural, dielectric and complex impedance properties of Cd doped SnO2 nanoparticles. J. Nanoeng. Nanomanuf. **3**(3), 229–236 (2013)

42. H.M. Alghamdi, A. Rajeh, Synthesis of CoFe2O4/MWCNTs nanohybrid and its effect on the optical, thermal, and conductivity of PVA/CMC composite as an application in electrochemical devices. J. Inorg. Organomet. Polym Mater. **32**(5), 1935–1949 (2022)

43. R. Nasser, W.B.H. Othmen, H. Elhouichet, Effect of Sb doping on the electrical and dielectric properties of ZnO nanocrystals. Ceram. Int. **45**(6), 8000–8007 (2019)

44. M.T. Ramesan, P. Jayakrishnan, T. Anilkumar, G. Mathew, Influence of copper sulphide nanoparticles on the structural, mechanical and dielectric properties of poly (vinyl alcohol)/poly (vinyl pyrrolidone) blend nanocomposites. J. Mater. Sci.: Mater. Electron. **29**(3), 1992–2000 (2018)

45. M.M. Abutalib, A. Rajeh, Boosting optical and electrical characteristics of polyvinyl alcohol/carboxymethyl cellulose nanocomposites by GNPs/MWCNTs fillers as an application in energy storage devices. Int. J. Energy Res. **46**(5), 6216–6224 (2022)

46. Q.A. Alsulami, A. Rajeh, Synthesis of the SWCNTs/TiO2 nanostructure and its effect study on the thermal, optical, and conductivity properties of the CMC/PEO blend. Results Phys **28**, 104675 (2021)

47. A. Arya, A.L. Sharma, Effect of salt concentration on dielectric properties of Li-ion conducting blend polymer

electrolytes. J. Mater. Sci.: Mater. Electron. **29**(20), 17903–17920 (2018)

48. M. Muthuvinayagam, C. Gopinathan, Characterization of proton conducting polymer blend electrolytes based on PVdF-PVA. Polymer **68**(1), 22–130 (2015)

Publisher's Note Springer Nature remains neutral with regard to jurisdictional claims in published maps and institutional affiliations.